Volume dependence of the Curie temperatures in diluted magnetic semiconductors

L. Bergqvist,[1] B. Belhadji,[1] S. Picozzi,[2] and P. H. Dederichs[1]
[1]*Institut für Festkörperforschung, Forschungszentrum Jülich, D-52425 Jülich, Germany*
[2]*Consiglio Nazionale delle Ricerche–Istituto Nazionale Fisica della Materia (CNR-INFM), 67010 Coppito, L'Aquila, Italy*
(Received 18 September 2007; published 15 January 2008)

Using electronic structure methods and statistical methods, we have studied theoretically the volume dependence of the exchange interactions and Curie temperatures in the diluted magnetic semiconductors. In both Mn-doped GaAs and Mn-doped InAs, the calculated Curie temperatures from numerical exact Monte Carlo simulations are more or less constant for a large volume interval. We have compared the exchange mechanisms in Mn-doped GaAs using both the local density approximation (LDA) and the LDA+U method. It is demonstrated that the magnetic properties are understood within Zener's p-d exchange model for the LDA+U, while in LDA they reflect a mixture between double and p-d exchange mechanisms.

DOI: 10.1103/PhysRevB.77.014418 PACS number(s): 75.50.Pp, 85.75.−d, 75.30.Et, 75.30.Hx

I. INTRODUCTION

The field of spintronics has attracted a great deal of attention during the last decade.[1–3] The possibility of combining the electronic charge and spin degrees of freedom opens up a new route to materials with new functionality, for instance, magnetic multilayers, which are used in giant magnetoresistance read heads in hard drives, diluted magnetic semiconductors (DMS), and half-metallic ferromagnets such as Heusler alloys. Half-metallic ferromagnets are particularly interesting due to the potential use as a spin injector in spintronics applications and have been intensively studied both theoretically and experimentally. Ever since the discovery of large-T_c ferromagnetism in Mn-doped GaAs by Ohno in 1998,[3] there has been very active research on different DMS systems.[4–7] Recent developments have made it possible to have more sophisticated control over defects in the samples. Moreover, annealing have increased the critical temperature T_C from around 110 to around 172 K for Mn-doped GaAs. Still, the T_C is well below room temperature, which prohibits a practical use of this material for devices, and there has been an active search for other DMS systems with room temperature ferromagnetism. Nevertheless, Mn-doped GaAs represents a very important playground for testing novel theoretical and experimental ideas due to the vast amount of data collected on this system. Moreover, the samples are usually very well characterized.

In this paper, we study the volume dependence of the critical temperature in Mn-doped GaAs and InAs theoretically using electronic structure methods and statistical methods. Despite the relative simplicity to study this experimentally, we have not found any experimental data for Mn-doped GaAs and InAs. However, for Mn-doped InSb, it has been shown that the system goes from a nonmagnetic material to a ferromagnetic material under pressure.[8] Theoretically, the volume dependence of the Curie temperatures has been recently reported for the half-metallic ferromagnets MnAs,[9] the Heusler alloy Ni_2MnSn,[10] and Fe-Co alloys.[11]

The paper is organized as follows: In Sec. II, we give details of the calculation procedure, Sec. III contains results from the calculations and discussions, and in Sec. IV we give our conclusions.

II. THEORY

A. Electronic structure

The electronic structure calculations were performed using the Korringa-Kohn-Rostoker (KKR) Green function method. Two different implementations of the KKR method were used. The first one employs the multipole-corrected atomic sphere approximation (ASA+M),[12] while the second is a full potential implementation of the KKR method. For more details about the full potential implementation, we refer to Ref. 13. Overall, the two implementations give very similar results. Empty spheres were included in the tetrahedral positions of the zinc blende lattice in order to obtain good space filling. Equal Wigner-Seitz radii were used for all spheres, and the valence basis set consists of *spdf* orbitals where scalar relativistic corrections are taken into account while spin-orbit effects are neglected. The energy levels of the core electrons are recalculated after each iteration by solving a fully relativistic Dirac equation. The effect of disorder was treated in the framework of coherent potential approximation (CPA). The local spin density approximation was employed for the exchange-correlation potential by using the parametrization of Perdew, Burke, and Ernzerhof.[14] We also performed some additional calculations based on the local density approximation (LDA)+U in order to check to what extent electron correlations affect our results. In these calculations, the Hubbard U parameter was fixed to 4 eV and the Hund exchange to 0.7 eV. The use of CPA in DMS systems was justified by comparing our CPA density of states and magnetic moments with supercell calculations using special quasirandom structures, where we find a very good agreement between the two methods.

B. Exchange interactions

If we neglect the very small direct interaction between Mn and As, the classical Heisenberg Hamiltonian in the zero external magnetic field can be written in the following form:

$$H = -\sum_{ij} J_{ij}\mathbf{e}_i \cdot \mathbf{e}_j, \tag{1}$$

where J_{ij} are Mn-Mn exchange interactions, i, j are unit cell indices, and $\mathbf{e}_i$ is the unit vector parallel to the magnetization

at site i. The positive (negative) values of J_{ij} correspond to the ferromagnetic (antiferromagnetic) couplings, respectively, and the magnitudes of the corresponding magnetic moments are included in the definition of J_{ij}. Small induced moments on the As and Ga atoms are not included in our description. The exchange interactions were obtained by mapping the electronic structure calculations to the classical Heisenberg Hamiltonian. Here, we employ the magnetic force theorem to calculate the energy change due to small rotation of the moment directions of the atoms at sites i and j.[15] In the framework of KKR-ASA-CPA the energy change could then be related to the exchange interaction by

$$\bar{J}_{ij} = -\frac{1}{8\pi i}\int_C \mathrm{Tr}_L[\Delta_i(z)\bar{g}_{ij}^{\uparrow}(z)\Delta_j(z)\bar{g}_{ji}^{\downarrow}(z)]dz. \quad (2)$$

Here, Tr_L denotes the trace over the angular momentum $L=(\ell m)$, $\Delta_i(z)=P_i^{\uparrow}(z)-P_i^{\downarrow}(z)$ is a diagonal matrix defined via the potential functions $P_i^{\sigma}(z)$ and is closely related to the exchange splitting corresponding to the magnetic atom, and $\bar{g}_{ij}^{\uparrow}(z)$ and $\bar{g}_{ji}^{\downarrow}(z)$ refer to site off-diagonal blocks of the conditionally averaged Green function, namely, the average over all configurations with a pair of magnetic atoms fixed at the sites i and j. The energy integration is performed along a contour in the complex energy plane, which encircles the occupied part of the valence band. The on-site exchange interaction J_0 of atom i could be directly calculated from the relation

$$\bar{J}_i^0 = \frac{1}{8\pi i}\int_C \mathrm{Tr}_L\{\Delta_i(z)[\bar{g}_{ii}^{\uparrow}(z)-\bar{g}_{ii}^{\downarrow}(z)] + \Delta_i(z)\bar{g}_{ii}^{\uparrow}(z)\Delta_i(z)\bar{g}_{ii}^{\downarrow}(z)\}dz, \quad (3)$$

where $\bar{g}_{ii}^{\sigma}(z)$ is the diagonal block of the conditionally averaged Green function.

C. Critical temperatures

The critical temperatures were evaluated using both the mean field approximation (MFA) and the more sophisticated Monte Carlo (MC) simulations. In the MFA, the critical (Curie) temperature T_C is proportional to the exchange interactions[15] as

$$k_B T_C^{MFA} = \frac{2}{3}xJ_0, \quad (4)$$

where $J_0 \approx \Sigma_j J_{0j}^{\text{Mn-Mn}}$, i.e., the sum of the Mn-Mn exchange interactions (in principle, J_0 also contains Mn-Ga and Mn-As contributions, but they are much smaller than the Mn-Mn contribution). x represents the concentration of magnetic atoms on the fcc lattice. It should be noted that the above expressions employ the so called virtual crystal approximation (VCA) or the averaged lattice in order to deal with diluted magnetic systems. It is known from earlier studies[16–19] that this approximation is very bad for diluted systems with localized exchange interactions where disorder and percolation effects play an important role. Therefore, we have also evaluated T_C using Monte Carlo simulations where both disorder and thermal fluctuations are properly included in a numerically exact procedure. The MC simulations employed the Metropolis algorithm where the critical temperature was evaluated by means of the cumulant crossing method.[20] In all cases, the lattice size was varied in order to employ finite size scaling, and the total number of magnetic atoms in the system was varied between 3000 and 15 000. Thirty disorder configurations were realized for each lattice size, and the thermal average of the magnetization was measured for around 30 000 Monte Carlo steps per lattice site.

III. RESULTS

Before we present results for the systems $Ga_{0.95}Mn_{0.05}As$ and $In_{0.95}Mn_{0.05}As$, we will first discuss the validity of the classical Heisenberg model and the use of the adiabatic approximation in the mapping for the present systems. The Heisenberg model as written in Eq. (1) only allows for transverse fluctuations of the spins (spin waves) and not any longitudinal fluctuations (Stoner excitations). In order to fulfill the validity, the spins must therefore be rigid under any rotation. For this purpose, we calculated the electronic structure in two different reference states, the ferromagnetic state and the disordered local moment (DLM) state. In both $Ga_{0.95}Mn_{0.05}As$ and $In_{0.95}Mn_{0.05}As$, the Mn local moment basically retains the same value for the two configurations, and one can conclude that the applicability of the Heisenberg model is justified for the present systems. It should be noted that we in the present study used the ferromagnetic (FM) reference state for the mapping. If instead the DLM reference state is used, the calculated critical temperature for $Ga_{0.95}Mn_{0.05}As$ using MC increases only by a few percent.

A. $Ga_{0.95}Mn_{0.05}As$

The system $Ga_{0.95}Mn_{0.05}As$ is definitely the most studied DMS system due to its rather high Curie temperature [172 K for 7% Mn (Refs. 5–7)], and it is rather well understood in many areas. However, as far as we know, no experimental data exist for the pressure dependence of the Curie temperature, which is studied here theoretically. In all the following, the experimental lattice constant a_{exp} refers to the value 5.65 Å.

1. Density of States

Figure 1(a) shows the calculated density of states of the Mn impurities for three different lattice constants ($\Delta a/a_{exp}=+3\%$, 0%, and -4%) using the local density approximation. For all lattice constants, a Mn impurity peak is present at the top of the valence band, being much weaker than the peak toward the bottom of the valence band. With increasing volume, the Mn density of states (DOS) narrows. This arises because of the hybridization with the valence p band, which strongly narrows since the p states become more localized. In parallel to this, the minority d peak moves to higher energies, from about 0.45 to 0.90 eV above E_F, which is directly related to an increase of the local moments.

Figure 1(b) shows the local DOS of Mn in (Ga,Mn)As with 5% Mn in the LDA+U approximation. Compared to the LDA results, the lower lying d peak is shifted from about

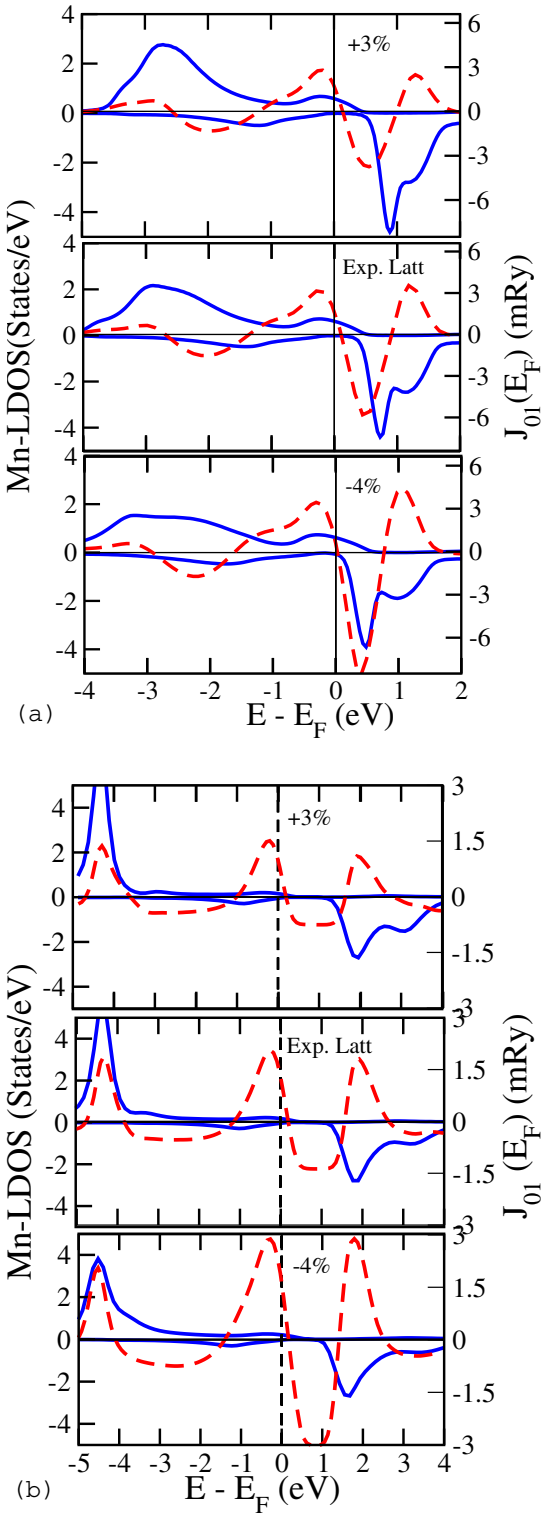

FIG. 1. (Color online) Local density of states (LDOS) (blue full line, left scale) of $Ga_{0.95}Mn_{0.05}As$ using the KKR method in the (a) LDA approximation and (b) LDA+U approximation. For each figure, the topmost panel corresponds to an expanded lattice (+3% of a_{exp}), the middle panel the experimental lattice, and the lowest panel a compressed lattice (−4% of a_{exp}). Here, a_{exp} denotes the experimental lattice constant. The dashed line (red, right scale) shows the exchange coupling constant J_{01} for nearest neighbor Mn impurity as a function of a fictitious value of the Fermi level E_F.

TABLE I. Mn and total magnetic moments of Mn-doped GaAs in LDA and LDA+U approximations and InAs in LDA.

System	$\Delta a/a_{exp}$	M_{loc}	M_{tot}
$(Ga_{0.95}Mn_{0.05})$ As (LDA)	+3%	3.85	4.00
	0%	3.70	4.00
	−4%	3.41	4.00
$(Ga_{0.95}Mn_{0.05})$ As (LDA+U)	+3%	4.43	4.34
	0%	4.29	4.25
	−4%	4.08	4.14
$(In_{0.95}Mn_{0.05})$ As (LDA)	0%	4.15	4.17

−3.0 eV to a sharp resonance at −4.2 eV, which is in very good agreement with experiments. At the same time, the resonance at E_F is considerably broadened, indicating a delocalization of the hole state. The low lying d peak shifts only slightly with volume. Due to the large U value, the minority peak above E_F is shifted by more than 1 eV to higher energies, depending again slightly on volume.

The delocalization of the hole state due to the Hubbard U parameter and the simultaneous shift of the majority d state to lower energies has the important consequence that the dominating exchange mechanism in LDA+U is Zener's p-d exchange,[21] while in LDA a mixture of double and p-d exchange determines the magnetic properties of (Ga,Mn)As.

2. Local and total moments

The local moments of Mn in (Ga,Mn)As are listed for three lattice constants in Table I, both in the LDA and the LDA+U method. In LDA, the local Mn moment increases from $3.41\mu_B$ for $\frac{\Delta a}{a_{exp}}=-4\%$ to $3.85\mu_B$ for $\frac{\Delta a}{a_{exp}}=+3\%$, reflecting the increased localization of the Mn wave function. In the whole volume range half-metallicity is preserved, yielding a constant total moment of $4\mu_B$ per Mn impurity.

Compared to the LDA, in LDA+U the calculated local moments of Mn are considerably larger, resulting from the increased localization of both the majority and the minority d-wave functions. At the same time, the pressure dependence becomes weaker. In addition, we obtain a total moment higher than $4\mu_B$, indicating that the majority and minority d-wave functions do not hybridize with the valence p states strongly enough to maintain half-metallicity.

3. Exchange coupling parameters and $J_{01}(E_F)$

In Fig. 2, the calculated coupling parameters J_{0j} are displayed as a function of the distance of impurity j from the onsite impurity at position 0. The results of LDA calculations, shown in Fig. 2(a), show a very different trend than the LDA+U results of Fig. 2(b). While these results show for all distances a steady increase of the interaction with compression, as one might expect from p-d exchange, the LDA values are rather insensitive to compression, except for the near-

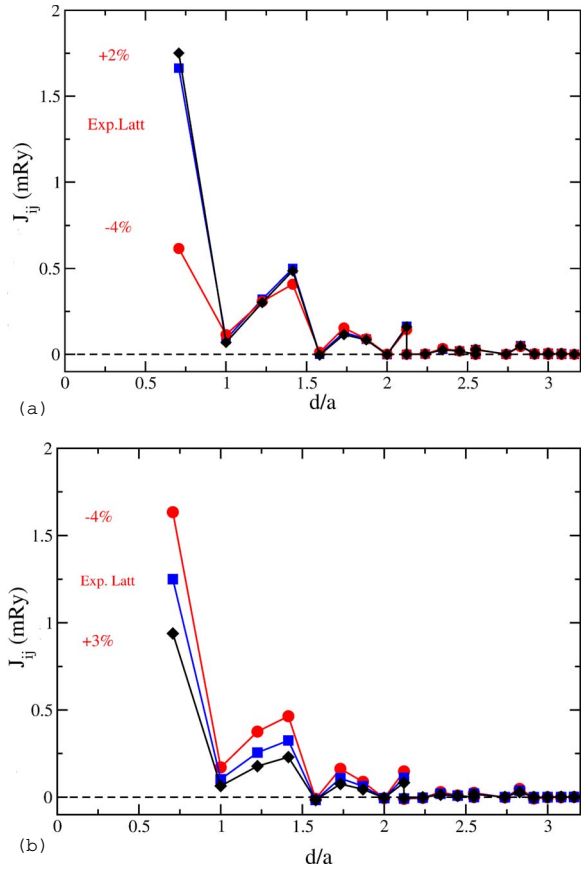

FIG. 2. (Color online) Calculated exchange interactions of $Ga_{0.95}Mn_{0.05}As$ using the KKR method in the (a) LDA approximation and (b) LDA+U approximation as a function of distance d (in units of lattice constant a).

est neighbor coupling constant, which for a 4% compression decrease by a factor of 3 and become negative for compressions larger than 5%.

This strong tendency toward antiferromagnetic coupling arises from super exchange, which basically varies as

$$\Delta E_{super} \sim c\frac{|t_{dd}|^2}{\Delta_{xs}}, \tag{5}$$

where c denotes the concentration, t_{dd} is the hopping matrix element between majority d states and minority d states of the impurity, and Δ_{xs} is the exchange splitting, being in LDA proportional to the local moment. Upon compression, t_{dd} increases, while at the same time Δ_{xs} decreases due to the reduction of the local moment. Usually, super exchange is very short ranged, affecting mostly the nearest neighbor couplings.

A clearer picture of the behavior of the different coupling mechanisms with compression can be obtained from Fig. 1, which shows in addition to the local DOS curve versus the energy E-E_F, also the exchange coupling constants $J_{01}(E_F^*)$ to the nearest neighbors as a function of an artificially changed Fermi level E_F^*, away from the self-consistent value of E_F. Both in LDA and LDA+U, these curves show three peaks close to E_F: First, a peak at around −0.3 eV arises due to p-d exchange and double exchange from the resonance at E_F. Second, the strongly negative value above E_F arises from the super exchange. Third, the positive peak at 1–2 eV above E_F arises from double exchange due to the minority d state in this energy region. The most important difference between the LDA and LDA+U is the much larger exchange splitting of $\sim U$, which shifts the majority peak down below −4 eV and, at the same time, the minority peak up by about 1.5 eV. Due to this, the exchange splitting in Eq. (5) is strongly increased, significantly reducing the super exchange in the energy gap region by as much as a factor of 4 since in LDA+U the exchange Δ_{xs} in Eq. (5) is given by the Hubbard U value. As a consequence, in LDA+U the super exchange is not important for the self-consistent J_{01} values in GaMnAs, whereas in LDA the J_{01} values strongly decrease with compression due to super exchange. Thus, in LDA the behavior of (Ga,Mn)As is determined by a complex superposition of double exchange, p-d exchange, *and* super exchange, while in the more realistic LDA+U approach, p-d exchange alone dominates the behavior, up to very strong compressions, where, finally, also in LDA+U super exchange will destabilize ferromagnetism.

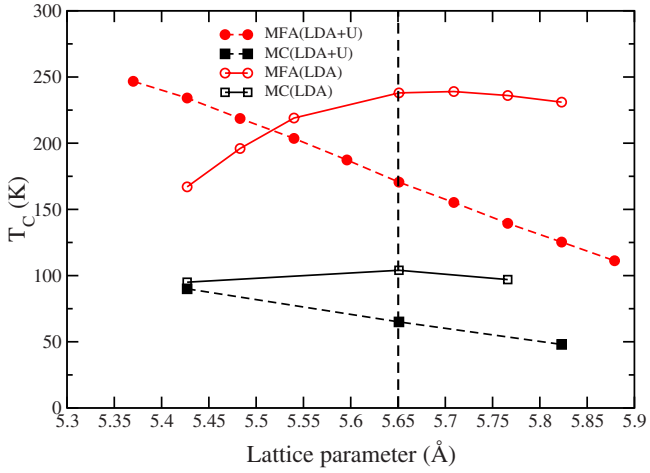

FIG. 3. (Color online) Calculated critical temperatures of $Ga_{0.95}Mn_{0.05}As$ in the LDA and LDA+U approximations. MFA-VCA denotes the mean field approximation in virtual crystal approximation, and MC the Monte Carlo results.

4. Critical temperatures

In Fig. 3, the calculated critical temperatures in $Ga_{0.95}Mn_{0.05}As$ using exchange interactions from the LDA and LDA+U approximations, are displayed. In the MFA, together with the VCA, all exchange interactions have the same weight, and due to the dominating nearest neighbor exchange interaction the values are very high. However, as have been demonstrated in several previous studies,[16–19] the MFA-VCA description is too oversimplified and cannot be applied to DMS systems. More specifically, the use of an average lattice (VCA) is not applicable to diluted systems. Instead, one has to rely on a lattice model where the Heisenberg model is solved numerically. Basically, two methods in this line have been developed: the local random phase ap-

proximation (LRPA)[18] and MC simulations. Here, we employ the Monte Carlo method, which, in principle, solves the spin fluctuations and disorder in the Heisenberg model exactly. One of the reason that the VCA description does not work for diluted systems is that the average separation between magnetic impurities is much larger than the nearest neighbor distance. For example, on a fcc lattice with 5% magnetic atoms, the average separation is slightly more than two lattice constants. Therefore, the thermodynamic quantities (T_C) are mainly determined by the exchange interactions around the average separation, and the nearest neighbor interactions do not carry much weight. Therefore, the calculated Curie temperatures from the MC simulations are much smaller than the MFA-VCA results. In LDA, the Curie temperatures from MC are basically constant around 100 K for the whole volume interval in $Ga_{0.95}Mn_{0.05}As$ (although a flat maximum is obtained for around the experimental lattice constant), while the results from the MFA-VCA show a distinct maximum for slightly expanded lattices due to the maximum of J_1 at this volume. In LDA+U, the calculated Curie temperatures increase slightly upon pressure, but overall the values are lower than the LDA results, in agreement with previous results.[17]

B. $In_{0.95}Mn_{0.05}As$

The system $In_{0.95}Mn_{0.05}As$ was chosen as its pressure dependence of the critical temperatures is a bit different from that of the $Ga_{0.95}Mn_{0.05}As$, as we will see below. The experimental lattice constant is 6.06 Å. All the following calculations were done using the LDA approximation.

1. Local moments and exchange parameters

For the three lattice constants (two compressed lattices with $\Delta a/a_{exp}=-6\%$ and -4% and for the experimental lattice constant), the calculated moments are given in Table I and the exchange coupling parameters J_{ij} are displayed in Figs. 4(a) and 4(b). The values are obtained by the LDA methods. Comparing with the LDA and LDA+U results for (Ga,Mn)As, we see that the LDA results for (In,Mn)As resemble more the LDA+U results for (Ga,Mn)As than the LDA results. Thus, even in LDA, the physical behavior is well described by p-d exchange. This is clearly shown in Fig. 4(a), where the interactions from the second to seventh cell show a monotonic increase with increasing pressure, and in Fig. 4(b), where the contributions of the different coordination shells to the mean field value of the critical temperatures are displayed ($n_{0j}J_{0j}$, where n_{0j} are the coordination number of shell j). However, the first nearest neighbors show a more complex behavior, and J_{01} has a maximum for -2% and slightly decreases for large compression, showing that also in (In,Mn)As super exchange becomes important.

2. Critical temperatures

The pressure dependence of the Curie temperatures is displayed in Fig. 5. Two different mean field estimates are shown, the first one is estimated from the Mn on-site exchange parameter J_0 and the second one from the Mn-Mn exchange interactions J_{ij}. The difference between the two

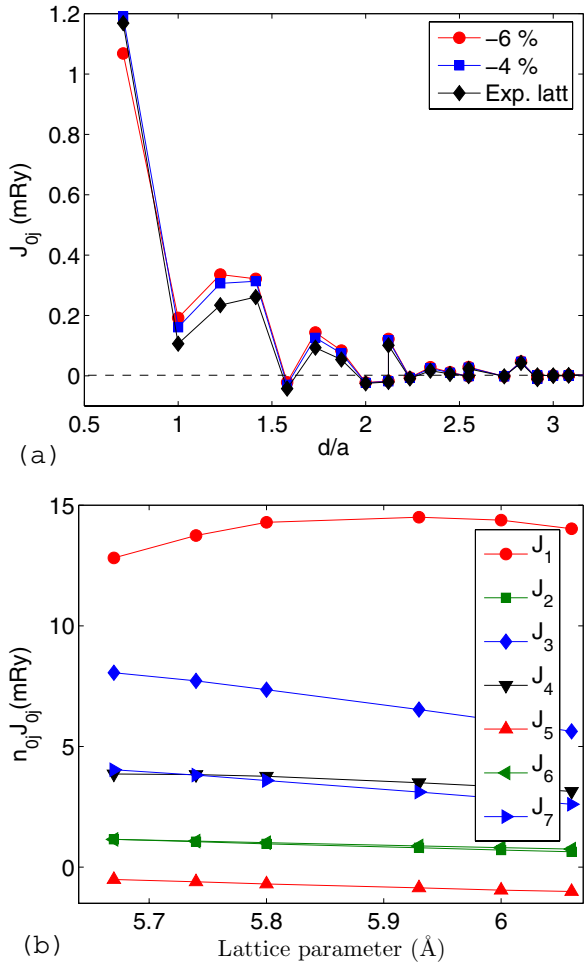

FIG. 4. (Color online) (a) Calculated exchange interactions of $In_{0.95}Mn_{0.05}As$ using the KKR method in the LDA approximation as a function of distance d (in units of lattice constant a). (b) Contribution to the mean-field critical temperatures for different coordination shells. The experimental lattice constant is 6.06 Å, corresponding to the last right value.

estimates are around 10% (which can be attributed to Mn-As, Mn-Ga, and Mn-interstitial contributions). Contrary to $Ga_{0.95}Mn_{0.05}As$ (in LDA), the critical temperatures increase with pressure, although the effect is rather weak. A similar kind of behavior has been observed in Mn-doped InSb,[8] which goes from a nonmagnetic material to a magnetic material (although with very low T_C) under pressure. This is very different from normal itinerant magnetic metals, which typically have a lower T_C when applying pressure. However, in rare-earth systems with localized 4f states, the opposite is true; i.e., they typically have an increasing T_C under pressure.

IV. DISCUSSION AND SIMPLE MODEL

In this section, we will further discuss the behavior of J_0 as a function of the lattice constant in both GaMnAs and InMnAs according to a simple model. We consider the coupling between (i) Mn d and host p states (responsible for the stabilization of the hole-induced FM spin arrangement via a

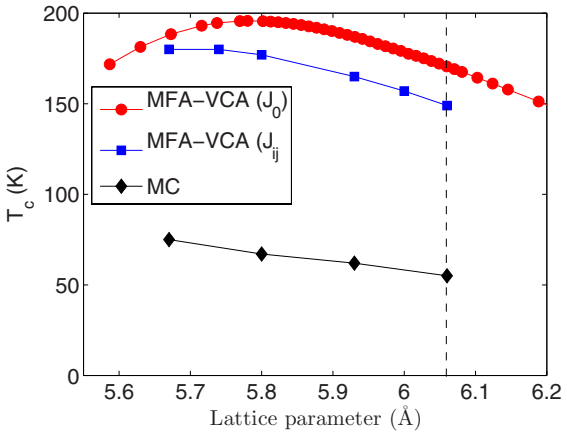

FIG. 5. (Color online) Calculated critical temperatures of $In_{0.95}Mn_{0.05}As$ in the LDA approximation. MFA-VCA denotes the mean field approximation in virtual crystal approximation (from both Mn on-site exchange parameter J_0 and Mn-Mn exchange interaction J_{ij}), and MC the Monte Carlo results.

Zener-like mechanism in narrow-gap semiconductors, such as InAs and, to a large extent, GaAs) and the (ii) Mn *d-d* interactions (responsible for the super-exchange mechanism that tends to stabilize an antiferromagnetic (AFM) spin configuration). It is well known that in DMS, symmetry favors the coupling between t_{2d} Mn states with t_{2p} valence states, giving rise to *p-d* delocalized hybrids, whereas the e_d states remain "nonbonding" with a much more localized character.

We here follow the model proposed by Dalpian *et al.*[22] along with their same notation: In the case of a valence band maximum lying between the majority and minority spin *d* states, as in GaMnAs and InMnAs, the total energy difference between the AFM and FM states can be expressed as

$$\Delta E(\mathrm{AFM}-\mathrm{FM}) = \alpha m_h(\Delta_{pd}^1 + \Delta_{pd}^2) - 6\Delta_{dd}^{1,2}, \qquad (6)$$

where $\alpha < 1$ is a prefactor related to the hole localization (i.e., it decreases when the hole states become more localized), m_h is the hole concentration, Δ_{pd}^1 and Δ_{pd}^2 represent the coupling between t_{2d} and t_{2p} states in the majority and minority spin channels, respectively, and $\Delta_{dd}^{1,2}$ represents the coupling between minority and majority spin *d* states (in turn, $\Delta_{dd}^{1,2}$ can be decomposed in two contributions, coming from t_2 and *e* electrons). In the above expression, the first term represents the Zener-like FM mechanism, whereas the second term represents the super-exchange AFM contribution. We extend this model in order to describe the dependence of J_0 [which is proportional to $\Delta E(\mathrm{AFM}-FM)$] on the lattice constant. In particular, each coupling parameter at the lattice constant *a* follows a "scaling law:" $\Delta_{ll'}(a) = \Delta_{ll'}(a_0) \times (a_0/a)^{n_{ll'}}$, where l, l' labels *p* and *d* orbitals, $\Delta_{ll'}(a_0)$ is the value of the coupling parameter at the equilibrium lattice constant a_0, and $n_{ll'}$ denote the exponents. This procedure follows the spirit of the semiempirical Slater-Koster approach to the tight-binding Hamiltonian for the dependence of the coupling terms on the interatomic distance; within this framework, the power dependence is generally denoted as Harrison-like scaling laws. Since the scaling power law is

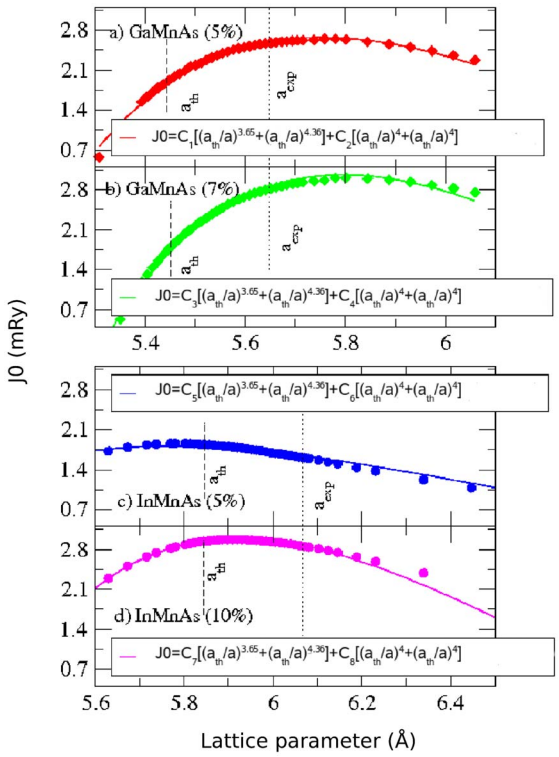

FIG. 6. (Color online) J_0 values calculated for (a) GaMnAs, 5%; (b) GaMnAs, 7%; (c) InMnAs, 5%; and (d) InMnAs, 10% (symbols). Solid lines show the fit according to the model. Vertical dashed (dotted) lines denote the theoretical (experimental) equilibrium lattice constants. $C_1 - C_8$ are proportionality constants.

expected to depend on the localization of the orbitals, in the fit we used different scaling exponents to describe the *p-d* coupling in the FM term, as well as the *d-d*(*e*) and *d-d*(t_2) couplings for t_2 and *e* states, respectively, in the AFM contribution. Here, we did not attempt to perform a full-tight-binding fit of all the parameters involved but only focused on modeling the pressure dependence of the coupling parameters that are relevant for the occurrence of a specific exchange mechanism. Therefore, the prefactor in front of the scaling laws contains all the terms, including the values of the hopping parameters at the equilibrium lattice constant, the proportionality constants, etc. The dependence of the coupling parameters on the lattice constant (both for the *p-d* coupling as well as for the *d-d* coupling) reflects what is expected: The *p-d* hybridization increases by applying pressure, so does the Zener mechanism. On the other hand, the exchange splitting is reduced by applying pressure; therefore, the minority states lie closer to the Fermi level (see the DOS plots shown in the previous sections), so that the super exchange is stronger for smaller lattice constants. This is equivalent to saying that as pressure is applied, the level repulsion between minority and majority *d* states increases since the coupling states get closer in energy. Therefore, both exchange mechanisms increase in module as a function of pressure; however, the final trend (i.e., nonmonotonous with a maximum in proximity to the equilibrium lattice constant) is determined by a competition of FM (positive) and AFM

(negative) effects, and the predominance of one over the other cannot be simply predicted without explicitly performing first-principles calculations.

Following a least-squares method, we have fitted the J_0 values as a function of the a lattice constant, and the results are shown in Fig. 6 for (a) GaMnAs, 5%; (b) GaMnAs, 7%; (c) InMnAs, 5%; and (d) InMnAs, 10%. The best fit resulted in a very high correlation coefficient and small rms error (>0.99 and ~ 0.02, respectively), showing that this simple model is sufficiently accurate to describe (not only qualitatively, but also quantitatively) the observed nonmonotonous trend as a function of pressure. Using the theoretically evaluated lattice constants [a_0(GaAs)$=5.44$ Å and a_0(InAs) $=5.86$ Å], the fitted exponents were 4, 3.65, and 4.36 for the p-d (both for spin-up and spin-down d states), d-$d(t_2)$, and d-$d(e)$ contributions, which are physically meaningful for scaling laws involving localized d states.[23]

V. CONCLUSIONS

In conclusion, we have presented the volume dependence of the exchange interactions for Mn-doped GaAs and InAs using both the LDA and the LDA$+U$ approximation. The exchange mechanisms in Mn-doped GaAs using LDA is a mixture between double and p-d exchange, while in LDA $+U$ the dominating exchange mechanism is Zener's p-d exchange. Mn-doped InAs is also well described within the p-d exchange mechanism.

The calculated exchange interactions were then subsequently used to estimate critical temperatures employing a classical Heisenberg model and numerically exact Monte Carlo simulations. In both systems, the critical temperatures stay rather constant in a large volume interval.

ACKNOWLEDGMENT

L.B. acknowledges support from the European Union (EU) in the framework of Marie Curie Actions for Human Resources and Mobility.

[1] S. Datta and B. Das, Appl. Phys. Lett. **56**, 665 (1990).
[2] G. Prinz, Science **282**, 1660 (1998).
[3] H. Ohno, Science **281**, 951 (1998).
[4] T. Dietl, Semicond. Sci. Technol. **17**, 377 (2002).
[5] K. W. Edmonds, K. Y. Wang, R. P. Campion, A. C. Neumann, C. T. Foxon, B. L. Gallagher, and P. C. Main, Appl. Phys. Lett. **81**, 3010 (2002).
[6] K. W. Edmonds, K. Y. Wang, R. P. Campion, A. C. Neumann, N. R. S. Farley, B. L. Gallagher, and C. T. Foxon, Appl. Phys. Lett. **81**, 4991 (2002).
[7] K. W. Edmonds, P. Boguslawski, K. Y. Wang, R. P. Campion, S. N. Novikov, N. R. S. Farley, B. L. Gallagher, C. T. Foxon, M. Sawicki, T. Dietl, M. B. Nardelli, and J. Bernholc, Phys. Rev. Lett. **92**, 037201 (2004).
[8] M. Csontos, G. Mihály, B. Jankó, T. Wojtowicz, X. Liu, and J. K. Furdyna, Nat. Mater. **4**, 447 (2005).
[9] B. Sanyal, O. Eriksson, and C. Aron, Phys. Rev. B **74**, 184401 (2006).
[10] E. Sasioglu, L. M. Sandratskii, and P. Bruno, Phys. Rev. B **71**, 214412 (2005).
[11] M. Lezaic, P. Mavropoulos, and S. Blügel, Appl. Phys. Lett. **90**, 082504 (2007).
[12] P. A. Korzhavyi, I. A. Abrikosov, B. Johansson, A. V. Ruban, and H. L. Skriver, Phys. Rev. B **59**, 11693 (1999).
[13] T. Huhne, C. Zecha, H. Ebert, P. H. Dederichs, and R. Zeller, Phys. Rev. B **58**, 10236 (1998).
[14] J. P. Perdew, K. Burke, and M. Ernzerhof, Phys. Rev. Lett. **77**, 3865 (1996).
[15] A. I. Lichtenstein, M. I. Katsnelson, V. P. Antropov, and V. A. Gubanov, J. Magn. Magn. Mater. **67**, 65 (1987).
[16] L. Bergqvist, O. Eriksson, J. Kudrnovský, V. Drchal, P. A. Korzhavyi, and I. Turek, Phys. Rev. Lett. **93**, 137202 (2004).
[17] L. Bergqvist, O. Eriksson, J. Kudrnovský, V. Drchal, A. Bergman, L. Nordström, and I. Turek, Phys. Rev. B **72**, 195210 (2005).
[18] R. Bouzerar, G. Bouzerar, and T. Ziman, Phys. Rev. B **73**, 024411 (2006).
[19] K. Sato, W. Schweika, P. H. Dederichs, and H. Katayama-Yoshida, Phys. Rev. B **70**, 201202(R) (2004).
[20] D. P. Landau and K. Binder, *A Guide to Monte Carlo Simulations in Statistical Physics* (Cambridge University Press, Cambridge, 2000).
[21] C. Zener, Phys. Rev. **81**, 440 (1950); **83**, 299 (1950).
[22] G. M. Dalpian, S. H. Wei, X. G. Gong, A. J. R. da Silva, and A. Fazzio, Solid State Commun. **138**, 353 (2006).
[23] L. Miglio and G. Malegori, Phys. Rev. B **52**, 1448 (1995).